Experimental study of the reaction $\pi^- p \rightarrow \Lambda K^0$ at beam momenta between 930 and 1130 MeV/c *

T. M. Knasel,† J. Lindquist, B. Nelson,‡ R. L. Sumner,§ E. C. Swallow, R. Winston, and D. M. Wolfe‖
Enrico Fermi Institute and Department of Physics, University of Chicago, Chicago, Illinois 60637

P. R. Phillips
Washington University, St. Louis, Missouri 63130

K. Reibel, D. M. Schwartz, and A. J. Stevens¶
Ohio State University, Columbus, Ohio 43210

T. A. Romanowski
Argonne National Laboratory, Argonne, Illinois 60439
and Ohio State University, Columbus, Ohio 43210

J. M. Watson
Argonne National Laboratory, Argonne, Illinois 60439
(Received 6 June 1974)

We have used an optical spark-chamber spectrometer to perform a systematic study of the reaction $\pi^- p \rightarrow \Lambda K^0$ at beam momenta between 930 and 1130 MeV/c. The cross section, angular distribution, and Λ polarization have been measured. We present our complete data from a sample of 11 400 events along with Legendre polynomial coefficients for the angular distributions. No striking cross-section enhancement at ΣK threshold is observed, but there is evidence for a small cusp effect. A simple model which takes account of the ΣK channel provides a good fit to our data.

The total and differential cross sections and the angular distribution of the polarization have been measured for the reaction $\pi^- p \rightarrow \Lambda K^0$ near the threshold for $\pi^- p \rightarrow \Sigma K$ (1033 MeV/c). We present here our complete data: sample A, 3000 events collected at 1025 MeV/c as a calibration for a study[1] of $\Lambda \rightarrow p e \bar{\nu}$, and sample B, 8400 events collected at 14 beam momenta between 930 MeV/c and 1130 MeV/c in a search for a cusp effect at ΣK threshold.[2]

It has been suggested by Wigner[3] and others[4-7] that, on the basis of the unitarity constraint, one should expect all channels to be influenced by the onset of a new channel. These threshold, or cusp, phenomena are usually small; however, some examples have been found in reactions with nuclei[8,9] and in $\pi\pi$ scattering at $K\bar{K}$ threshold.[10] Several experiments[11-15] have studied the reaction $\pi^- p \rightarrow \Lambda K^0$ near ΣK threshold; however, the results are inconclusive. In the most recent experiments, Van Dyck *et al.*[15] found a cross-section enhancement about 10 MeV/c below threshold; while in another experiment, Jones *et al.*[14] saw no effect. We observe a small dip in the $\pi^- p \rightarrow \Lambda K^0$ cross section, $\sigma(\Lambda K)$, and a corresponding increase in the Λ production asymmetry at ΣK threshold. We have fitted our data with a simple model based on the $S_{11}(1700)$ πN resonance. Inclusion of the effect of the ΣK threshold results in good agreement with the observed structure.

I. PION BEAM

The experiment was performed at the Argonne National Laboratory Zero Gradient Synchrotron (ZGS). Negative pions were produced by 12-GeV proton interactions in a beryllium target. A two-stage configuration of magnets (Fig. 1) was used to select momentum and focus the negative beam on a 2.54-cm. diameter liquid hydrogen target. The beam momentum (near 1025 MeV/c) was calibrated for several magnet current settings with a positive beam by measuring the π^+-deuteron time-of-flight difference and the deuteron range.[16] The uncertainty in the central momentum from these measurements, including energy loss straggling in the hydrogen target, was ± 3 MeV/c. Other beam momenta were obtained by linearly scaling the field of the second bending magnet and tuning the first to maximize the beam incident on the target.

The momentum acceptance was controlled by an adjustable collimator at the first focus of the beam transport system (see Fig. 1). The momentum acceptance for data sample A was ± 12 MeV/c, and for sample B was ± 6 MeV/c, including energy

loss in the hydrogen target. A CO_2 gas Cherenkov counter inside the last quadrupole magnet was used to veto the 20% electron component of the beam. The muon component of the beam was measured to be 3% at 1025 MeV/c.[17] Typically the instantaneous beam rate for samples A and B was 1.0 ± 0.2 and 0.3 ± 0.5 MHz, respectively.

II. EVENT DETECTION AND TRIGGERING

The apparatus (Fig. 2) consisted of a liquid hydrogen target surrounded by a veto counter and imbedded in an array of optical spark chambers immersed in the field of a magnet with 100 cm gap.[18] Counters on either side of the magnet detected the $\Lambda \to p\pi^-$ decay products. Above ΣK threshold we detected Λ's from $\pi^- p \to \Sigma^0 K^0$ ($\Sigma^0 \to \Lambda\gamma$) in addition to directly produced Λ's from $\pi^- p \to \Lambda K^0$. The $\Sigma^0 K^0$ events were separated by kinematic analysis.

A beam telescope ($\overline{C1} \cdot B1 \cdot B2 \cdot B3 \cdot \overline{B4}$) and the target veto counter (T) selected pion interactions in the target which resulted in neutral final states (neutrals). Protons from Λ decay were detected in counter $P1$ and in the 7-element hodoscopes $P2$ and $P3$. A water Cherenkov counter ($C2$) was used in anticoincidence to reject fast particles; e.g., positrons from γ conversion or π's from K^0 decays. The proton momentum, typically 600 MeV/c, was analyzed by the field in the magnet gap (central value 5.73 kG). The Λ-decay pion was detected in the 6-element hodoscope (EH) on the opposite side of the magnet, and its momentum, typically 100 MeV/c, was analyzed in the magnet's fringe field. Our three trigger components thus were : (neutral production) $= \overline{C1} \cdot B1 \cdot B2 \cdot B3 \cdot \overline{B4} \cdot \overline{T}$, (proton)$= P1 \cdot P2 \cdot P3 \cdot \overline{C2}$, and (pion)$= EH$. These three requirements—neutral production, a slow particle on the proton side of the magnet, and one particle on the pion side—combined to provide an effective trigger for the spark chambers.

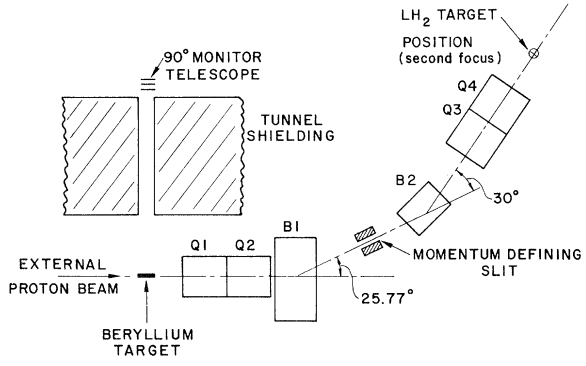

FIG. 1. Beam transport system. The intensity of protons incident on the beryllium target just upstream of $Q1$ was monitored by the "90°" counter telescope. An adjustable collimator located at the first focus determined the momentum acceptance.

III. DATA COLLECTION

The plan and elevation views of the spark chambers were recorded on 35-mm film through independent optical systems[18] with a 90° stereo angle. Fiducials were located at 5-cm intervals alongside each chamber and used to eliminate large-scale optical distortions. A data box, photographed simultaneously, contained the frame and run numbers and lights indicating which hodoscope counters were involved in the event trigger.

The time of flight for each of the Λ-decay products was recorded by photographing two 4-gun cathode-ray tubes.[19] A pulse pair was displayed corresponding to signals from each end of the 6 EH and 7 $P2$ counters. An initial time marker was taken from beam counter $B2$ (see Fig. 2). The time scale was calibrated with a 50-MHz sine wave once every 100 frames, and zero-time constants were established using e^+e^- pairs ($\beta = 1$). The time-of-flight resolution after removing path length differences was ± 1 nsec.

The events in data sample A were collected along with $\Lambda \to pe\bar{\nu}$ data during several long running periods. The beam momentum for this data was 1025 MeV/c. Data sample B was obtained in two weeks of running, during which background and beam rates were quite uniform. As a safeguard against systematic errors, three passes

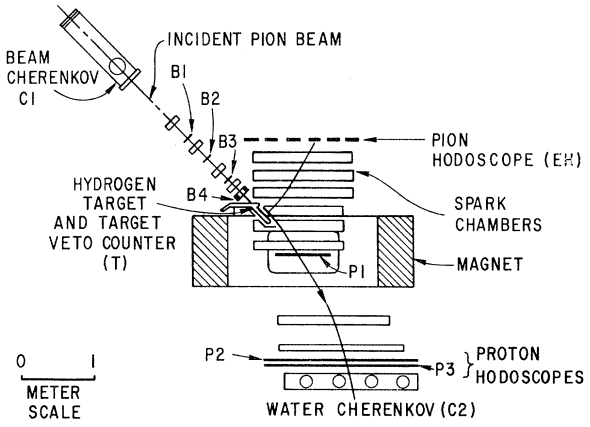

FIG. 2. Plan view of the apparatus showing a typical $\Lambda \to p\pi^-$ event. The gas Cherenkov counter $C1$ was used to veto electrons in the beam. Counter $B4$ has a 2.54-cm hole and was used in anticoincidence. The trigger requirements are: neutral production $= \overline{C1} \cdot B1 \cdot B2 \cdot B3 \cdot \overline{B4} \cdot \overline{T}$, proton$= P1 \cdot P2 \cdot P3 \cdot \overline{C2}$, and pion$= EH$.

were made over the momentum interval 930 to 1130 MeV/c. Calibration and background information was obtained from data taken with the beam momentum set below ΛK^0 threshold, and at several momenta with the target empty. Beam-track pictures were used to measure the average length of beam particles in the target, and cosmic-ray pictures were used to check the alignment of the spark chambers.

IV. DATA PROCESSING

The film was scanned twice. Scanners were instructed to look for vees—events consisting of a pair of tracks having the correct charge and originating in a specified region around the target. It was also required that these tracks could be extrapolated to within half a counter width to the hodoscope counter which produced the event trigger. This double scan found vees in about 20% of the frames with an efficiency > 96%. A typical pair of spark-chamber pictures is shown in Fig. 3.

At this point, the film for sample B went directly to be spark measured (see below) while that for sample A was processed in parallel with the $\Lambda\beta$ data. For data sample A, the 8-gun oscilloscope film was measured on image plane digit-

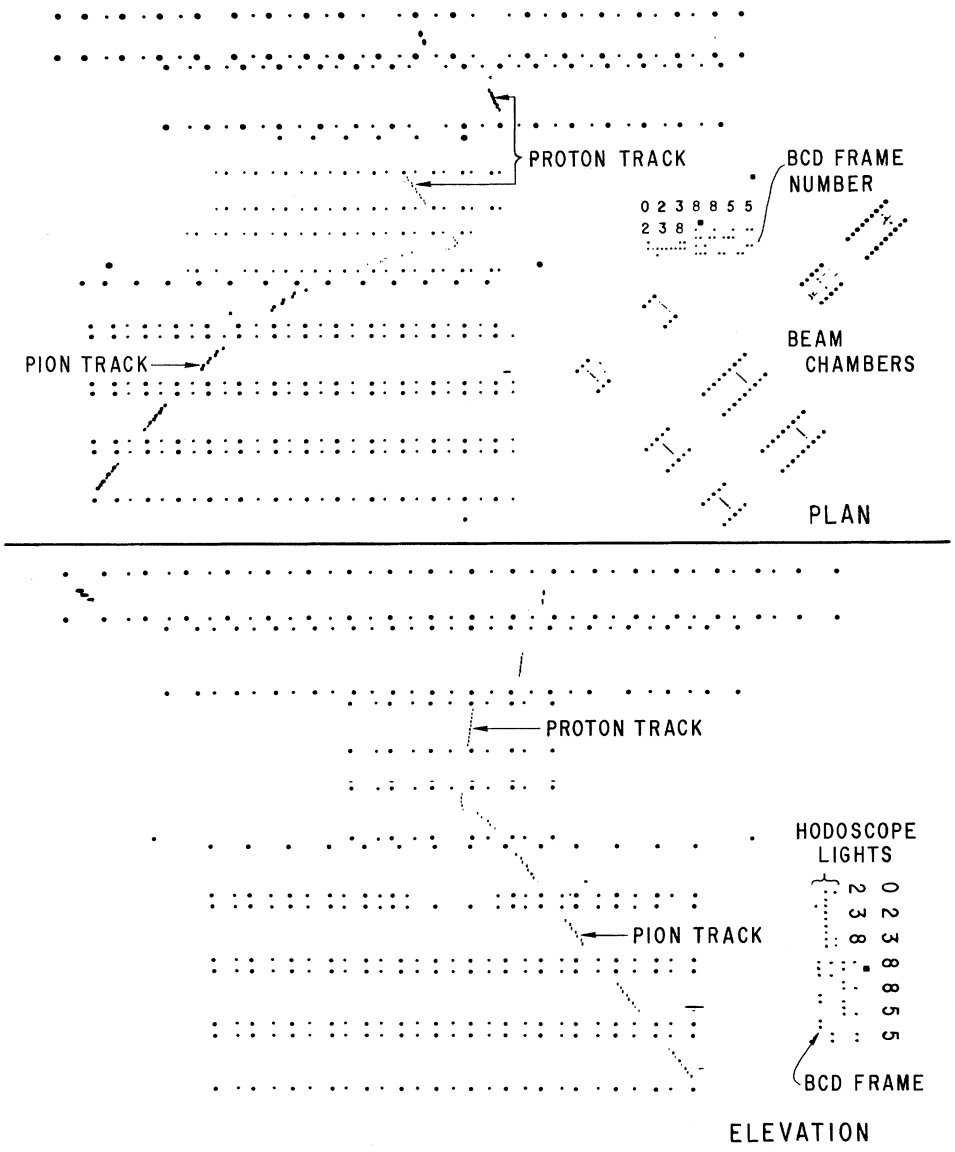

FIG. 3. Plan and elevation view spark-chamber picutres. Images of several chambers have been displaced to fit within our 35-mm film format.

izers. A cut was imposed on the positive-particle time of flight to reject positrons. Typically 75% of the frames survived this cut with a loss of less than 4% of the $\Lambda p\pi$ events. The spark-chamber film was measured on image plane digitizers with a least count of 0.007 cm (real space equivalent).

For data sample B, vees found by the scanners were digitized by Alice,[20] a general-purpose flying spot scanner coupled to a PDP-10 computer at the Argonne National Laboratory Applied mathematics Division. The film was measured in two passes, the second of which was aided by a hand-drawn sketch of the correct sparks to ensure high measuring efficiency (> 96%). Beam tracks were measured only for those frames which contained a single unobscured beam track. About 20% of the events did not have a beam track measurement, and the appropriate correction has been applied in the cross-section calculation.

For both samples A and B spatially reconstructed spark positions along the two tracks of the vee were fit simultaneously to determine the particle momenta.[21] In this procedure the tracks were required to have a common vertex. The χ^2 minimization procedure included the effects of spark and fiducial measuring errors, multiple Coulomb scattering, spark staggering, and momentum loss (assuming the particles to be a proton and π^-).

V. EVENT SELECTION

During the scanning and measuring process essentially all the nonvee frames were eliminated. The remaining sample of $\Lambda p\pi$ events, e^+e^- pairs, and $\pi^- p$ scatters were subjected to the criteria listed in Table I. The three constraint quantities for $\pi^- p \to \Lambda K^0$ were taken to be the invariant mass of the vee (assuming π^- and p), the momentum of the Λ transverse to the production plane, and the missing mass recoiling from the Λ. Histograms of these quantities are shown in Fig. 4. The missing-mass plot in Fig. 4 shows the separation of ΛK^0 and $\Sigma^0 K^0$ events. A cut on the missing mass at 535 MeV/c results in less than 2% contamination of the ΛK^0 sample by $\Sigma^0 K^0$ events. Comparison of our value for the K^0 mass with the present

TABLE I. Criteria used in selection of events.

(1) Decay fiducial volume outside the target veto counter.

(2) Decay products must not intersect the target veto counter.

(3) Decay-pion range greater than the distance to the pion hodoscope.

(4) Decay-pion momentum ≤170 MeV/c.

(5) $\pi^- p$ effective mass between 1090 and 1140 MeV/c^2.

(6) One measured beam track.

(7) Momentum of the Λ transverse to the production plane ≤70 MeV/c.

(8) Production vertex in the target fiducial volume.

(9) Missing mass at the production vertex,
(a) between 460 and 535 MeV/c^2 for $\pi^- p \to \Lambda K^0$;
(b) greater than 535 MeV/c^2 for $\pi^- p \to \Sigma^0 K^0$.

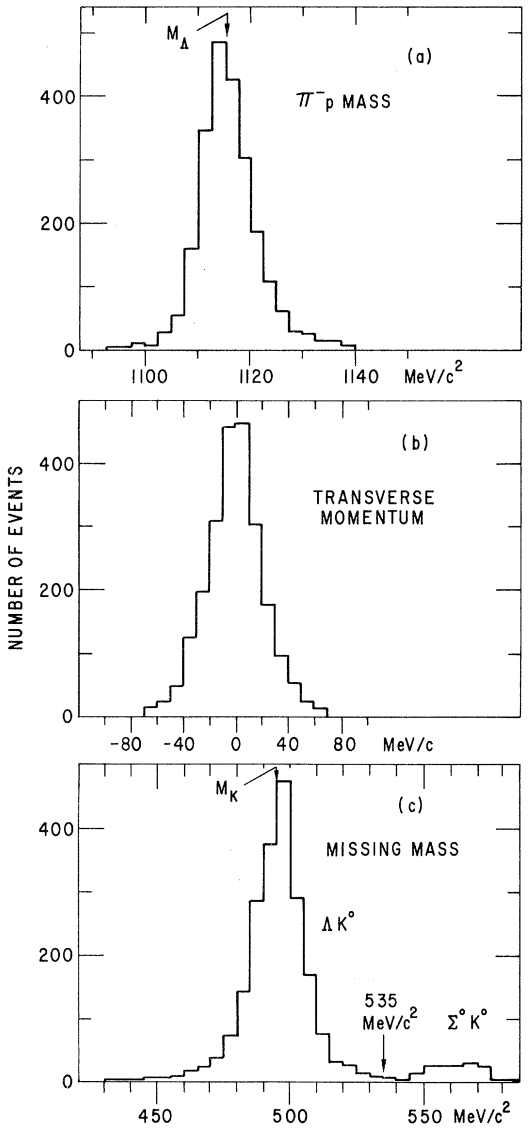

FIG. 4. Constraint quantities: (a) Pion-proton invariant mass; (b) momentum of the Λ transverse to the production plane; and (c) the missing mass recoiling from the Λ. A cut at 535 MeV/c^2 in the missing mass is used to separate ΛK^0 and $\Sigma^0 K^0$ events.

world average confirms our beam momentum calibration to within ± 3 MeV/c.

VI. CROSS SECTIONS

In determining total cross sections, the data from sample A were not used because of the uncertainty in the normalization. However, for determination of the angular distributions and polarizations samples A and B are treated identically.

From the incident pion flux and the "neutrals" counting rate, we have calculated the cross section for $\pi^- p \to$ all neutral final states:

$$\sigma(\text{neutrals}) = \frac{N}{B^*} \frac{1}{n l_T \Omega_N} - (\text{target empty}) . \quad (1)$$

Here n is the target density (0.42×10^{23} protons/cm^3), l_T is the total length of hydrogen (35 cm), Ω_N is the "neutral" detection efficiency and is 1 in this experiment, the number of "neutral" counts is N, and the number of effective beam pion counts is B^*. Data taken at seven momenta with the target empty determined the nonhydrogen rates which we subtracted. In determining B^* we have included the following corrections: random anticoincidences (10%), π^- interaction losses including δ rays which hit the target anticounter (20%), beam divergence effects (20%), and muon contamination (3%).[17] The resulting cross sections are compared with those from other experiments in Fig. 5 (see Refs. 22–28). Our statistical errors are negligible; however, there is an overall uncertainty in the above corrections of about $\pm 5\%$. The agreement of our cross sections with the world's data indicates the reliability of our calculation of the effective pion flux.

Our $\pi^- p \to \Lambda K^0$ cross section is calculated from

$$\sigma(\Lambda K) = \frac{N_{\Lambda K}}{B^*} \frac{1}{n l \Omega_{\Lambda K}} Q - (\text{target empty}) . \quad (2)$$

The number of ΛK^0 events is $N_{\Lambda K}$, B^* is the effective pion flux including the corrections discussed above for the neutrals cross section, l is the length of hydrogen in the production fiducial volume, and Q is a correction for scanning and measuring losses (5%) and for events without a measured beam track (20%). The detection efficiency $\Omega_{\Lambda K}$ was determined by a Monte Carlo simulation which took account of the effects of the triggering geometry, target escape efficiency, momentum loss, multiple Coulomb scattering, and decays in the flight of the pion. The efficiency for the Λ to escape from our target is a sensitive function of the Λ lifetime. We have used a lifetime value of $\tau^0 = 0.25$ nsec. The following empirical formula can be used to adjust the cross sections presented here for a revised value of the Λ lifetime, τ:

$$\frac{\sigma - \sigma^0}{\sigma^0} = - \frac{10.2}{(p - 897)^{0.324}} \frac{\tau - \tau^0}{\tau^0} ,$$

where p is the laboratory beam momentum in MeV/c. For the branching ratio $(\Lambda \to p\pi^-)/(\Lambda \to \text{all states})$ we have used 0.640 ± 0.005. The resulting cross sections, together with those from other experiments, are shown in Fig. 6(a) (see Refs. 29–34). Our values are given in Table II. Our quoted errors are statistical only; however, we estimate that there is a $\pm 15\%$ uncertainty in the over-all normalization. The uncorrected yield of Λ's from $\pi^- p \to \Sigma^0 K^0$ is shown in Fig. 7.

VII. POLARIZATION AND ANGULAR DISTRIBUTIONS

Parity conservation in the production process requires that the Λ's may only be polarized along the normal to the production plane, $\hat{n} \equiv \hat{\Lambda} \times \hat{\pi}$. In the parity-violating decay $\Lambda \to p\pi$ the angular distribution of the proton with respect to the Λ spin is

$$f(\phi) = \tfrac{1}{2}(1 + \alpha P \cos\phi) , \quad (3)$$

where α is the decay asymmetry parameter[35]; P is the Λ polarization, and $\cos\phi \equiv \hat{n} \cdot \hat{p}$, where $\hat{p}$ is a unit vector along the decay-proton direction. To cancel symmetric biases, we have estimated αP by the ratio of moments[36]

$$\alpha P = \langle \cos\phi \rangle / \langle \cos^2\phi \rangle . \quad (4)$$

In this way the polarization $P(\cos\theta)$ was determined in each of 10 production cosine bins. ($\cos\theta$

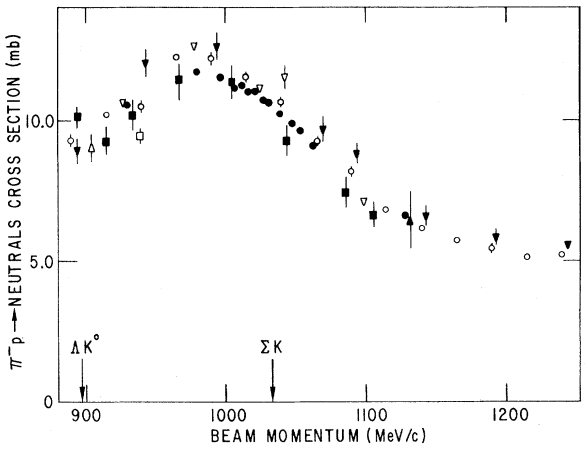

FIG. 5. Cross section for $\pi^- p \to$ neutrals (all neutral final states). Our statistical errors are negligible; however, we estimate the uncertainty in the over-all normalization to be $\pm 5\%$. The data are from the following sources: □, Ref. 22; △, Ref. 23; ○, Ref. 24; ▽, Ref. 25; ■, Ref. 26, ▲, Ref. 27; ▼, Ref. 28; and ●, this experiment.

$\equiv \pi \cdot K$ in the production center-of-mass system.) Our Monte Carlo simulation shows no appreciable bias on αP (i.e., <0.02). Comparison of αP calculated from Λ's produced to the left (spin up) and from those produced to the right (spin down) also shows no bias.

Our Monte Carlo simulation gives the detection efficiency for all values of $\cos\theta$ and is used to correct for bias in the observed angular distributions. The efficiency functions are shown in Fig. 8 for several beam momenta. The corrected differential cross section, $\sigma(\theta)$, is normalized to the integrated cross section calculated above and is given in Table II together with the product $\sigma(\theta)P(\theta)$. Also given is the average polarization defined as

$$\langle P\rangle = \int \sigma(\theta)P(\theta)d\Omega \Big/ \int \sigma(\theta)d\Omega\,, \tag{5}$$

and the production asymmetry, $A_{\Lambda K} = 2(B-F)/(B+F)$, where B and F are the numbers of Λ's going either backward or forward in the production center-of-mass system. The cross section, average Λ polarization, and the production asymmetry are shown in Fig. 6.

The angular distributions expanded in Legendre polynomials are

$$\sigma(\theta) = \sum_{l=0} A_l P_l \tag{6}$$

and

$$\sigma(\theta)P(\theta) = \sum_{l=1} B_l P_l^1\,. \tag{7}$$

These have been independently fitted for A_l and B_l, with $l \leq 3$; higher terms are not significantly different from zero. The coefficients are given in Table III and are compared with the data of Doyle[33] and Binford *et al.*[32] in Figs. 9(a) and 9(b).

VIII. AMPLITUDE ANALYSIS

We observe no large enhancement in the ΛK^0 cross section; however, just at ΣK threshold, we do observe a small dip in the cross section and a simultaneous increase in the backward-forward asymmetry (see Fig. 6). These changes occur over too small a momentum interval to be directly associated with known πN resonances whose widths are typically 100 MeV. These narrow features can be associated with the isospin-$\frac{1}{2}$ ΣK cross section which increases rapidly from threshold and is approximately equal to the ΛK^0 cross section 35 MeV/c above threshold. The conditions necessary for interference of the $I=\frac{1}{2}$ ΣK amplitude and the ΛK^0 S-wave amplitude are met as follows: (a) the $I=\frac{1}{2}$ ΣK system is an S wave near threshold[12]; (b) the ΛK^0 system is pure isospin $\frac{1}{2}$, and is about 50% S wave near ΣK threshold[37-39]; and (c) the $\Lambda\Sigma$ relative parity is even.[40]

Several previous analyses[37-39] of $\pi^- p \to \Lambda K^0$ have found the dominant amplitudes to be resonant S_{11}

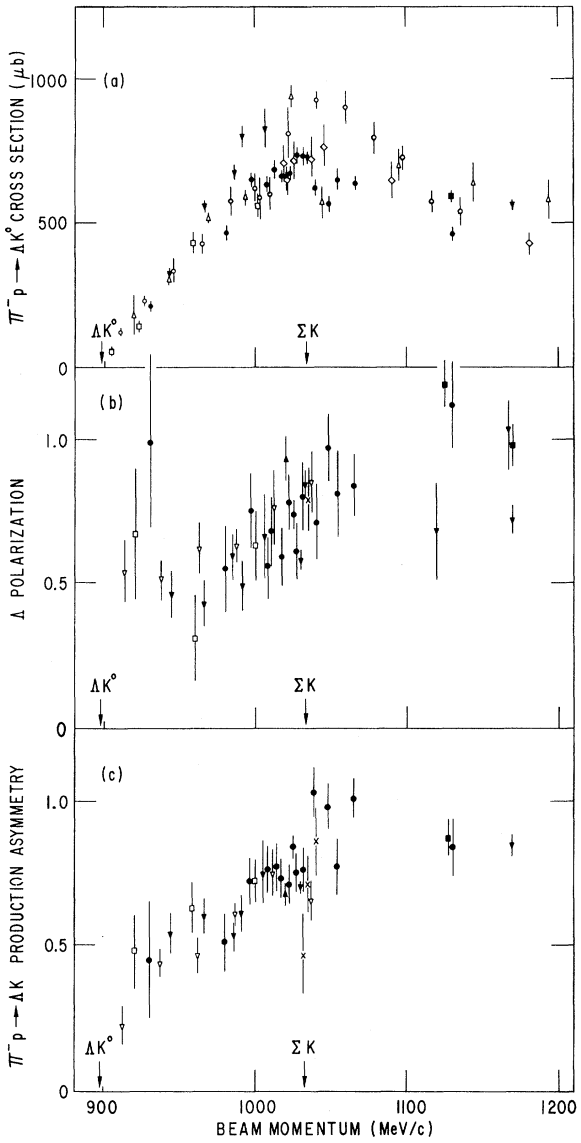

FIG. 6. (a) The $\pi^- p \to \Lambda K^0$ cross section; (b) the average Λ polarization; and (c) the backward-forward production asymmetry, $A_{\Lambda K}$. Our quoted errors are statistical; however, there is an additional uncertainty of 15% in the over-all cross-section normalization. The data are taken from the following sources: ▽, Ref. 30; □, Ref. 29; ■, Ref. 32; ▼, Refs. 12, 33, and 34; ×, Ref. 11; △, Ref. 15; ◇, Ref. 31; ○, Ref. 14; ▲, Ref. 13; and ●, from this experiment.

TABLE II. Summary of cross sections, angular distributions, and polarizations for data sample A (1025 MeV/c) and sample B (other momenta). No cross section was determined for sample A; here $\sigma(\theta)$ is normal to sample B. The quoted error is statistical; in addition, there is a 15% uncertainty in the cross-section normalization.

$\cos\theta$ \ (MeV/c)	930 ± 6		980 ± 6		997 ± 6		1007 ± 6		1012 ± 6		1017 ± 6		1022 ± 6		1025 ± 12	
	σ	$\Delta\sigma$	σ	$\Delta\sigma$	σ	$\Delta\sigma$	σ	$\Delta\sigma$	σ	$\Delta\sigma$	σ	$\Delta\sigma$	σ	$\Delta\sigma$	σ	$\Delta\sigma$
0.95	19.4	12.6	79.4	23.1	116.7	30.9	85.7	23.5	90.3	26.0	116.5	27.8	90.2	23.2	134.4	23.3
0.85	38.0	17.2	51.7	14.7	78.0	18.2	72.1	15.4	113.0	21.2	86.3	15.5	110.9	17.4	93.8	9.2
0.75	42.6	16.5	55.4	13.4	71.2	14.9	67.6	12.7	120.8	18.6	110.7	15.0	102.6	14.0	112.0	8.3
0.65	21.9	10.1	42.7	10.3	65.6	12.7	91.9	13.3	68.2	12.3	87.5	11.8	68.4	10.1	90.4	6.2
0.55	18.7	8.5	46.8	10.0	69.6	12.2	68.4	10.7	77.5	12.3	64.8	9.5	85.5	10.7	78.3	5.3
0.45	13.3	6.7	40.3	8.7	62.0	11.0	67.9	10.2	63.4	10.7	65.7	9.2	66.1	9.1	68.1	4.8
0.35	18.6	7.7	46.4	9.1	68.1	11.2	75.3	10.6	64.7	10.6	44.5	7.4	49.2	7.7	48.7	3.9
0.25	24.0	8.6	36.8	7.9	47.6	9.3	52.0	8.7	54.1	9.7	40.8	7.1	42.2	7.1	61.0	4.4
0.15	12.0	6.1	28.4	7.0	49.6	9.5	55.4	9.0	47.9	9.1	58.4	8.5	50.0	7.8	47.8	3.9
0.05	6.2	4.4	30.8	7.3	70.8	11.6	40.7	7.8	47.4	9.2	56.1	8.5	54.9	8.3	57.7	4.3
−0.05	12.9	6.5	51.6	9.8	56.5	10.5	36.1	7.5	45.4	9.2	42.5	7.5	59.3	8.8	41.9	3.7
−0.15	13.7	6.9	43.0	9.1	39.4	8.9	36.1	7.6	56.7	10.5	38.9	7.3	45.8	7.8	50.5	4.2
−0.25	11.0	6.4	37.6	8.8	24.9	7.2	34.6	7.6	51.5	10.2	56.1	9.0	42.4	7.7	43.7	3.9
−0.35	19.6	8.9	25.3	7.4	46.2	10.2	45.4	9.1	44.1	9.7	23.8	6.0	47.8	8.4	35.5	3.7
−0.45	16.7	8.5	36.0	9.2	33.0	8.9	28.2	7.4	29.3	8.2	41.5	8.3	39.0	7.9	39.0	4.0
−0.55	17.7	9.0	19.4	6.9	33.4	9.4	32.9	8.3	22.3	7.5	42.3	8.8	31.1	7.4	31.8	3.8
−0.65	14.0	8.3	13.2	6.0	31.5	9.6	30.2	8.5	25.3	8.5	28.2	7.6	21.8	6.7	31.9	4.1
−0.75	0.0	6.9	14.8	6.7	19.8	8.2	38.2	10.5	33.4	10.8	21.7	7.4	16.8	6.4	23.3	3.9
−0.85	16.7	10.1	17.5	8.0	20.0	9.1	10.1	5.9	12.6	7.3	24.5	8.9	27.8	9.5	11.7	3.1
−0.95	13.4	10.3	13.5	8.1	26.1	12.5	13.3	8.0	11.0	8.0	20.2	9.6	8.2	5.9	12.6	4.0
$\cos\theta$	σP	$\Delta\sigma P$	σP	$\Delta\sigma P$	σP	$\Delta\sigma P$	σP	$\Delta\sigma P$	σP	$\Delta\sigma P$	σP	$\Delta\sigma P$	σP	$\Delta\sigma P$	σP	$\Delta\sigma P$
0.90	−5.1	25.7	10.2	31.0	41.9	40.7	26.6	31.9	13.2	38.8	30.1	33.7	66.3	33.9	45.1	15.6
0.70	29.5	26.3	40.2	23.0	42.9	26.3	69.4	25.0	80.9	30.8	57.7	24.6	53.7	22.8	82.4	10.6
0.50	−13.1	15.1	55.8	19.7	50.4	22.7	45.6	20.1	53.1	22.7	41.5	17.7	76.3	20.1	62.4	7.8
0.30	37.3	18.0	44.1	17.2	61.6	21.1	31.2	18.2	63.1	20.5	39.1	14.5	57.7	15.4	55.7	6.7
0.10	7.1	10.5	29.4	14.2	44.3	20.6	47.6	17.2	20.7	17.3	56.2	17.1	44.7	15.9	47.3	6.7
−0.10	−9.9	13.1	24.7	17.9	15.4	18.5	9.0	14.2	49.6	19.4	10.3	13.9	78.0	18.0	31.8	6.1
−0.30	16.3	15.2	18.9	15.7	48.5	18.0	−12.3	15.7	75.7	22.1	26.0	15.0	37.0	15.9	37.3	6.1
−0.50	44.5	22.6	15.3	15.7	29.3	18.0	24.5	15.2	12.7	15.1	28.1	16.6	16.4	14.3	21.2	6.1
−0.70	25.9	24.2	−0.8	12.1	13.1	17.0	28.8	18.2	20.6	18.3	2.0	13.9	0.7	12.2	25.1	6.7
−0.90	41.8	26.8	−36.9	19.7	38.2	22.1	5.5	12.8	−21.8	17.5	26.1	18.2	−19.2	16.4	3.3	5.0
Events	83		323		433		531		479		657		684		2994	
$\sigma(\Lambda K)$ (μb)	212 ± 23		467 ± 26		652 ± 31		634 ± 28		686 ± 31		665 ± 26		675 ± 26		...	
$\langle P \rangle$	0.99 ± 0.30		0.55 ± 0.15		0.75 ± 0.13		0.56 ± 0.12		0.68 ± 0.12		0.59 ± 0.10		0.78 ± 0.10		0.74 ± 0.05	
$A_{\Lambda K}$	0.45 ± 0.20		0.51 ± 0.10		0.72 ± 0.08		0.76 ± 0.08		0.77 ± 0.08		0.73 ± 0.07		0.71 ± 0.07		0.84 ± 0.04	

$\cos\theta$ \ (MeV/c)	1027 ± 6		1031 ± 6		1039 ± 6		1048 ± 6		1054 ± 6		1065 ± 6		1130 ± 6	
	σ	$\Delta\sigma$	σ	$\Delta\sigma$	σ	$\Delta\sigma$	σ	$\Delta\sigma$	σ	$\Delta\sigma$	σ	$\Delta\sigma$	σ	$\Delta\sigma$
0.95	106.9	26.7	114.9	32.1	114.7	32.2	96.6	26.4	105.1	34.4	129.2	33.9	72.1	20.5
0.85	107.0	17.3	135.0	23.3	109.5	20.2	115.2	17.9	118.4	23.6	125.7	18.3	78.8	13.5
0.75	86.8	13.0	88.4	15.7	100.7	16.5	63.5	10.9	111.8	19.8	78.1	11.9	79.9	12.4
0.65	89.3	11.9	83.8	13.9	74.2	12.8	69.5	10.6	59.8	13.3	102.5	12.9	60.7	10.7
0.55	99.6	11.9	92.4	13.9	72.5	12.2	56.8	9.2	92.0	16.2	82.8	11.2	54.0	10.6
0.45	75.3	10.0	82.3	12.8	71.7	11.9	85.8	11.3	42.5	10.8	60.6	9.5	31.3	8.6
0.35	68.7	9.4	50.7	9.9	74.5	12.0	46.8	8.2	37.2	10.0	61.1	9.5	39.2	10.5
0.25	55.0	8.4	62.1	10.9	46.7	9.4	48.3	8.3	53.4	12.1	42.0	7.8	26.6	9.1
0.15	53.3	8.3	40.0	8.8	39.7	8.7	50.2	8.5	35.0	9.8	47.7	8.4	43.7	12.1
0.05	57.1	8.7	58.4	10.8	38.4	8.7	45.1	8.1	62.3	13.2	39.3	7.6	27.5	9.4
−0.05	57.5	8.9	36.0	8.5	41.2	9.1	28.6	6.5	57.4	12.7	47.8	8.4	25.5	8.7
−0.15	51.2	8.5	64.0	11.6	36.3	8.6	27.7	6.4	66.7	13.8	28.3	6.4	38.7	10.3
−0.25	39.0	7.6	36.5	8.9	35.5	8.7	33.1	7.1	45.6	11.5	43.3	8.1	26.0	8.0

TABLE II. *(Continued)*

$\cos\theta$ \ (MeV/c)	1027 ± 6		1031 ± 6		1039 ± 6		1048 ± 6		1054 ± 6		1065 ± 6		1130 ± 6	
	σ	$\Delta\sigma$	σ	$\Delta\sigma$	σ	$\Delta\sigma$	σ	$\Delta\sigma$	σ	$\Delta\sigma$	σ	$\Delta\sigma$	σ	$\Delta\sigma$
−0.35	33.5	7.2	40.8	9.7	28.5	8.0	29.9	7.0	17.9	7.3	36.0	7.5	35.6	9.1
−0.45	36.1	7.8	60.8	12.4	32.9	8.9	21.9	6.1	31.9	10.2	32.1	7.3	15.3	5.9
−0.55	29.0	7.3	37.7	10.2	26.0	8.3	14.9	5.3	21.1	8.7	19.4	6.0	18.1	6.5
−0.65	37.6	9.0	21.7	8.3	9.0	5.2	29.9	8.2	36.3	12.3	14.2	5.4	12.3	5.6
−0.75	30.4	9.0	37.5	12.1	7.2	5.1	12.8	5.8	9.7	6.9	12.1	5.5	11.2	5.7
−0.85	35.7	11.2	4.8	4.8	9.2	6.5	9.7	5.7	18.2	10.7	12.1	6.2	16.0	7.4
−0.95	12.9	7.7	25.2	13.3	11.9	8.7	20.9	10.1	15.6	11.4	7.6	5.6	10.0	6.0
$\cos\theta$	σP	$\Delta\sigma P$	σP	$\Delta\sigma P$	σP	$\Delta\sigma P$	σP	$\Delta\sigma P$	σP	$\Delta\sigma P$	σP	$\Delta\sigma P$	σP	$\Delta\sigma P$
0.90	16.8	30.8	13.9	44.0	2.1	41.2	87.1	35.8	103.8	50.8	41.6	35.3	59.4	28.5
0.70	39.4	20.3	97.3	29.9	83.7	28.9	55.8	20.4	55.0	32.2	76.4	23.0	109.6	24.9
0.50	84.2	19.8	98.9	27.0	44.3	23.0	63.0	19.5	83.3	29.1	80.6	20.9	45.5	19.5
0.30	32.8	15.7	60.0	21.1	46.2	21.1	48.3	16.3	28.9	21.3	53.9	17.4	68.4	23.8
0.10	53.0	15.1	42.8	19.4	36.9	17.2	68.7	17.7	35.1	22.3	30.9	15.3	29.9	21.3
−0.10	15.5	15.1	58.2	20.5	55.2	19.1	31.8	13.2	65.2	26.5	56.9	16.3	38.0	19.1
−0.30	25.4	13.4	17.6	17.6	36.0	17.2	48.7	15.4	9.3	18.2	56.6	16.9	40.5	17.7
−0.50	31.7	13.9	38.1	22.3	32.5	17.6	19.5	11.8	36.0	20.2	27.5	13.8	−1.6	11.6
−0.70	32.5	16.3	7.1	19.4	10.5	10.8	14.4	13.6	11.9	19.2	5.8	10.2	5.1	10.5
−0.90	25.4	18.0	32.7	19.4	−1.7	14.2	0.6	14.5	−8.4	20.8	−1.0	10.7	9.7	13.0
Events	709		475		413		526		318		618		314	
$\sigma(\Lambda K)$ (μb)	737 ± 28		734 ± 34		620 ± 31		568 ± 25		651 ± 37		640 ± 26		462 ± 26	
$\langle P\rangle$	0.61 ± 0.10		0.80 ± 0.12		0.71 ± 0.13		0.97 ± 0.12		0.81 ± 0.15		0.84 ± 0.11		1.12 ± 0.15	
$A_{\Lambda K}$	0.75 ± 0.07		0.76 ± 0.08		1.03 ± 0.09		0.98 ± 0.08		0.77 ± 0.10		1.01 ± 0.07		0.84 ± 0.10	

and P_{11} waves with smaller $J=\frac{3}{2}$ (either P_{13} or D_{13}) amplitudes. The $J=\frac{5}{2}$ amplitudes appear to be very small. We assume that the $S_{11}(1700)$ resonance decays to both ΛK^0 and $|\Sigma K, I=\frac{1}{2}\rangle$ states and treat the threshold effect in a manner similar to Flatté *et al.*[10] and Votava and Thompson.[8] The ΛK^0 S-wave amplitude (with no background terms) is

$$S_{\Lambda K}=(\Gamma_{\pi p}\Gamma_{\Lambda K})^{1/2}/[2(E_R-E)-i\Gamma_T], \qquad (8)$$

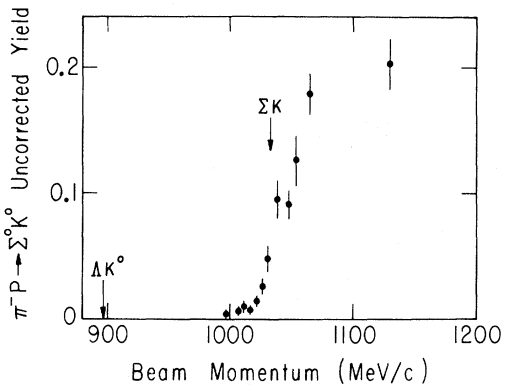

FIG. 7. Uncorrected yield of Λ's from $\pi^- p \to \Sigma^0 K^0$.

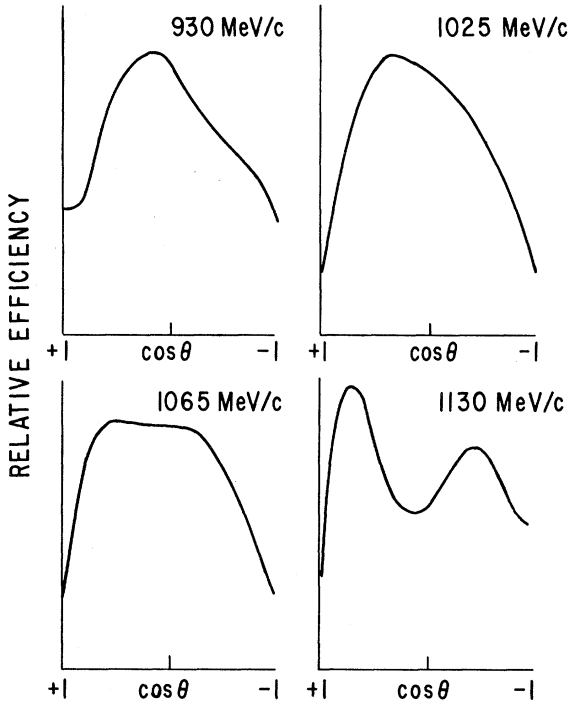

FIG. 8. The detection efficiency of our apparatus as a function of cosθ for several beam momenta.

TABLE III. Legendre polynomial coefficients as determined by a least-squares fit with $l \leq 3$. The 1025-MeV/c entries are from data sample A; all others are from sample B. In these fits we used 20 points in $\sigma(\theta)$ and 10 points in $\sigma(\theta)P(\theta)$ so there are 16 degrees of freedom for A_l and 7 for the B_l.

Momentum (MeV/c)	A_1/A_0	A_2/A_0	A_3/A_0	χ^2/DF	B_1/A_0	B_2/A_0	B_3/A_0	χ^2/DF
930	0.34 ± 0.26	0.54 ± 0.29	0.18 ± 0.34	0.48	1.10 ± 0.36	0.46 ± 0.32	0.46 ± 0.26	1.77
980	0.68 ± 0.13	0.01 ± 0.16	0.15 ± 0.17	0.82	0.74 ± 0.16	0.40 ± 0.13	−0.11 ± 0.11	0.72
997	0.71 ± 0.11	0.10 ± 0.14	0.00 ± 0.16	0.86	0.92 ± 0.15	0.17 ± 0.12	0.10 ± 0.11	0.68
1007	0.80 ± 0.10	0.08 ± 0.12	0.04 ± 0.13	0.96	0.65 ± 0.13	0.30 ± 0.11	0.18 ± 0.09	1.03
1012	0.88 ± 0.10	0.17 ± 0.13	0.19 ± 0.13	0.76	0.90 ± 0.15	0.27 ± 0.12	−0.09 ± 0.10	1.85
1017	0.81 ± 0.09	0.34 ± 0.11	0.26 ± 0.12	1.45	0.72 ± 0.12	0.23 ± 0.10	0.09 ± 0.09	0.86
1022	0.85 ± 0.09	0.17 ± 0.11	0.29 ± 0.11	1.11	1.03 ± 0.13	0.39 ± 0.10	−0.11 ± 0.09	0.97
1025	0.92 ± 0.05	0.27 ± 0.06	0.32 ± 0.06	2.16	0.91 ± 0.05	0.31 ± 0.04	0.09 ± 0.03	1.22
1027	0.81 ± 0.08	0.19 ± 0.11	0.07 ± 0.11	0.61	0.73 ± 0.15	0.15 ± 0.12	0.13 ± 0.11	0.47
1031	0.99 ± 0.10	0.26 ± 0.13	0.40 ± 0.15	1.58	0.95 ± 0.13	0.35 ± 0.11	0.16 ± 0.09	0.81
1039	1.15 ± 0.11	0.30 ± 0.14	0.11 ± 0.15	0.64	0.91 ± 0.15	0.23 ± 0.12	−0.03 ± 0.09	0.61
1048	0.98 ± 0.10	0.27 ± 0.13	0.02 ± 0.14	1.24	1.22 ± 0.14	0.39 ± 0.12	0.03 ± 0.10	0.90
1054	0.98 ± 0.14	0.33 ± 0.17	0.30 ± 0.18	1.92	0.99 ± 0.19	0.39 ± 0.16	0.12 ± 0.14	1.14
1065	1.12 ± 0.10	0.38 ± 0.12	0.23 ± 0.12	0.97	1.07 ± 0.12	0.35 ± 0.10	−0.01 ± 0.08	1.10
1130	1.00 ± 0.12	0.41 ± 0.16	0.23 ± 0.16	0.79	1.35 ± 0.19	0.73 ± 0.14	0.20 ± 0.12	1.28

where the total width Γ_T represents a sum over all decay channels: πp, ΛK^0, ΣK, and so on. The ΣK partial width is given by

$$\Gamma_{\Sigma K} = \begin{cases} b|q| & \text{above threshold} \\ ib|q|e^{-|\xi q|} & \text{below threshold,} \end{cases} \tag{9}$$

where q is the momentum in this channel. The factor $e^{-|\xi q|}$ has been introduced to provide reasonable damping below threshold.[41] The proportionality constant b is fixed by the known $|\Sigma K, I=\frac{1}{2}\rangle$ cross section (550 μb at 1080 MeV/c).[42]

Higher partial-wave amplitudes are parameterized as Breit-Wigner resonances with a slowly varying background:

$$f_l = e^{i\phi}(\Gamma_{\pi p}\Gamma_{\Lambda K})^{1/2}/[2(E_R - E) - i\Gamma_T] + q^{2l+1}(C_1 + C_2 q + \cdots). \tag{10}$$

Here we have followed the example of Orito and Sasaki[38] except that we have included an over-all phase ϕ for each resonance.[39]

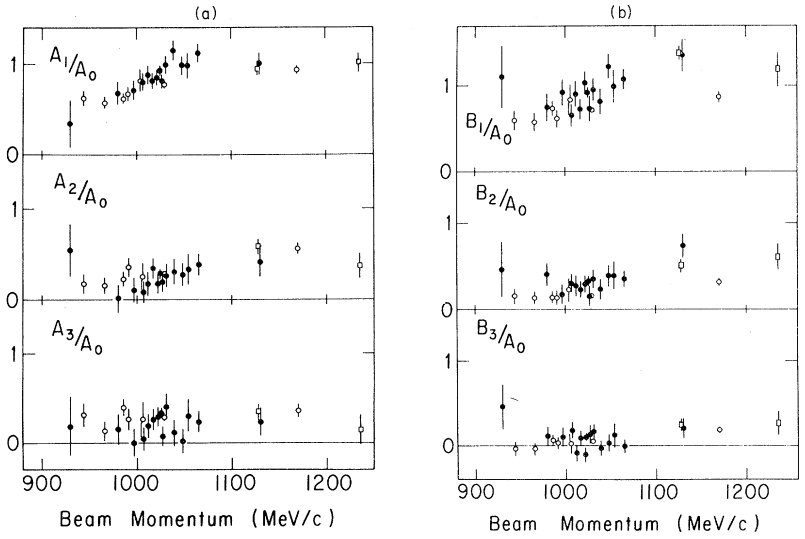

FIG. 9. (a) Legendre polynomial coefficients for $\sigma(\theta)$. (b) Legendre coefficients for $\sigma(\theta)P(\theta)$. Open circles are from Ref. 33, the open squares from Ref. 32, and the closed circles are the values from this experiment.

We have found χ^2 minima corresponding to two initial assumptions for the relevant amplitudes: (I) S_{11}, P_{11}, and P_{13}; and (II) S_{11}, P_{11}, and D_{13}. In addition, each of these solutions also contains small $J=\frac{5}{2}$ background amplitudes. Only the data from this experiment were used in the χ^2 minimization.[43] There were 30 values of $\sigma(\theta)$ and $\sigma(\theta)P(\theta)$ at each of 15 beam momenta for a total of 449 data points. (The normalization for data sample A was taken from sample B.) Typically 11 parameters were varied to find *a priori* reasonable solutions; that is, we required S_{11} and P_{11} to be the dominant amplitudes.

The two solutions (corresponding to I and II above) have χ^2 values of 460 and 463 with confidence levels of 23% and 20%, respectively. The values of the parameters for solutions I are given in Table IV (see Refs. 39 and 44) and are quite similar to those of Refs. 38 and 39. The cross section, production asymmetry, and polarization calculated from the partial-wave amplitudes for solutions I and II are shown by the solid curves in Figs. 10 and 11. Both solutions show a dip in $\sigma(\Lambda K)$ and a corresponding increase in $A_{\Lambda K}$ at ΣK threshold. However, while solution I follows the increasing trend of the Λ polarization with the beam momentum, solution II does not.

Solutions excluding the cusp are found by setting $\Gamma_{\Sigma K}=0$ reminimizing χ^2. The resulting χ^2 values are 522 and 516, with confidence levels of 0.34% and 0.63% for solutions I and II, respectively. These solutions are shown by the dashed curves in Figs. 10 and 11. As anticipated, these solutions do not reproduce the structure seen in the data at ΣK threshold.

This model, which uses reasonably well established resonance parameters and includes the ΣK channel, qualitatively reproduces the observed structure in $\sigma(\Lambda K)$ and $A_{\Lambda K}$ with a substantial improvement in χ^2. We note that, except for the small effect of the ξ parameter, inclusion of the ΣK channel introduces no additional freedom into the model as $\Gamma_{\Sigma K}$ is fixed by the $|\Sigma K, I=\frac{1}{2}\rangle$ cross section.

Recently reported preliminary results from an experiment studying the reactions $\pi^- p \to \Lambda K$ and $\pi^- p \to \Sigma^0 K^0$ $(\Sigma^- K^+)$ (Ref. 45) with statistical accuracy comparable to ours show a similar dip in the cross section and a somewhat smaller increase in the asymmetry.

ACKNOWLEDGMENTS

We wish to express our gratitude to the staff of the ZGS Complex at Argonne National Laboratory, and in particular to E. Hayes, J. Terandy, C. Rush, J. Upton, and D. Burant. We thank

TABLE IV. Partial-wave parameters. The first column gives our parameters for solution I including the cusp. In the second column are E_R, Γ_T, and $\Gamma_{\pi p}/\Gamma_T$ from the πN analysis of Almehed and Lovelace (Ref. 44). For $(\Gamma_{\pi p}\Gamma_{\Lambda K})^{1/2}/\Gamma_T$, we give the range of values from Wagner and Lovelace (Ref. 39). Partial widths are evaluated at the resonance energy. For this solution $\xi=1.0$ F; and $\chi^2=460$.

	S_{11}		P_{11}		P_{13}		D_{13}		D_{15}		F_{15}	
	Our fit	Refs. 39,44	Our fit	Refs. 39,44	Our fit	Refs. 39,44	Our fit	Refs. 39,44	Our fit	Refs. 39,44	Our fit	Refs. 39,44
E_R (MeV)	1675	1670	1670	≈1720	1850	≈1850	0	1520	0	1683	1685	1688
Γ_{tot} (MeV)	170	120	174	≈160	327	≈300	0	120	0	150	155	140
$\Gamma_{\pi p}$ (MeV)	30		36		85		0		0		105	
$\Gamma_{\Lambda K}$ (MeV)	15		8.2		20		0		0	<0.2	0.02	<0.1
$\Gamma_{\Sigma K}$ (MeV)	40											
$\Gamma_{\pi p}/\Gamma_{\text{tot}}$	0.18	0.33	0.21	0.13	0.26	≈0.17	0	0.39	0	0.30	0.68	0.43
$(\Gamma_{\pi p}\Gamma_{\Lambda K})^{1/2}/\Gamma_{\text{tot}}$	0.12	0.17 to 0.19	0.10	0.13 to 0.17	0.13	≈0.10	0	~0.08	0		0.01	
ϕ	0°		70°		31°		0°		0°		37°	
Background												
100 C_1	0		0		0		0		$0.11 \pm 0.08i$		0	
100 C_2	0		0		0		0		0		0	

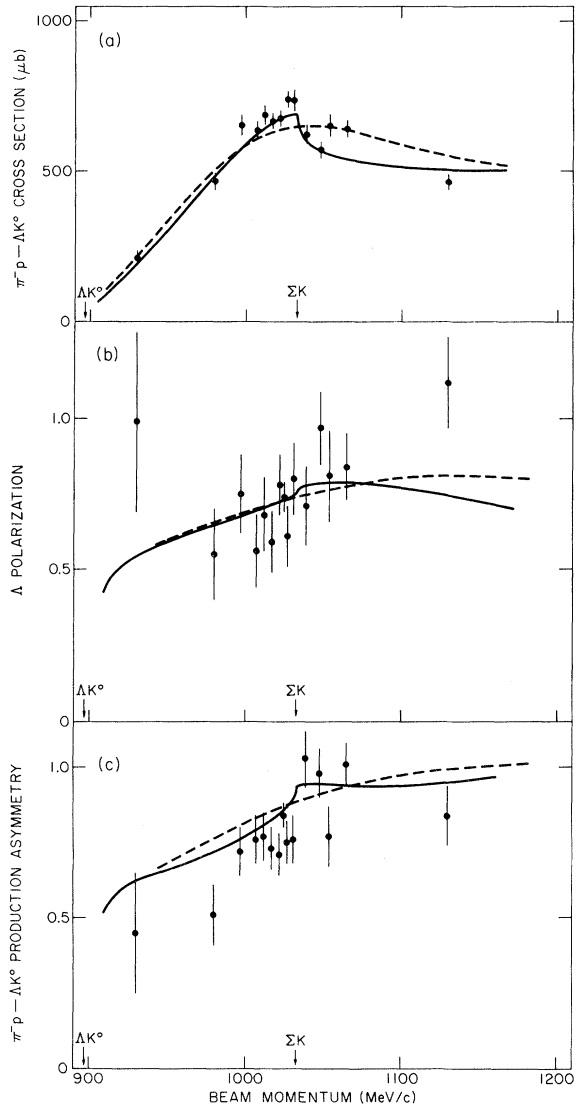

FIG. 10. Solution I compared to data from this experiment. The solid line represents solution I including the cusp at ΣK threshold, and the dashed line represents the result of minimizing χ^2 with $\Gamma_{\Sigma K}=0$ (no cusp).

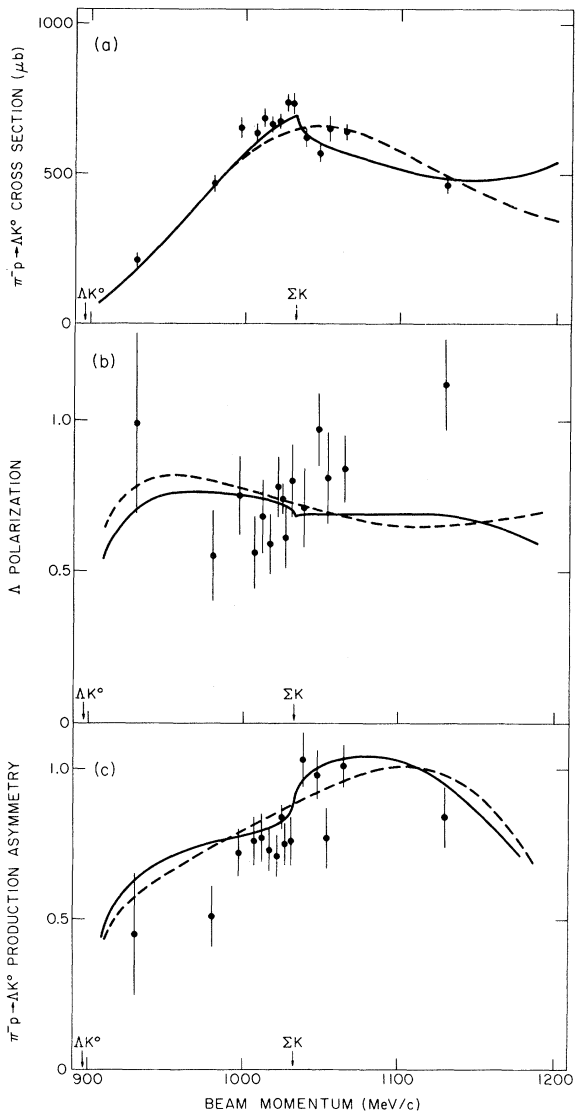

FIG. 11. Solution II compared to data from this experiment. The solid line represents solution II including the cusp at ΣK threshold, and the dashed line represents the result of minimizing χ^2 with $\Gamma_{\Sigma K}=0$ (no cusp).

O. Van Dyck, S. Frankel, G. Snape, and W. Flatté of the University of Pennsylvania for showing us their data before publication. The hospitality and cooperation of the Argonne National Laboratory Applied Mathematics Division, and the assistance of D. Hodges, B. Kroupa, R. Wehman and J. Haasl, is gratefully acknowledged. We are also grateful to S. Watson for help with the data analysis and to the scanners and measurers at the University of Chicago and Ohio State University.

---

*Research supported in part by the U. S. Atomic Energy Commission, the National Science Foundation, and the Louis Block Fund of the University of Chicago.

†Present address: Science Applications, Inc., 1651 Old Meadow Road, Mclean, Virginia 22101.

‡Present address: Department of Physics, University of Illinois, Urbana, Illinois 61801.

§Work submitted in partial fulfillment of the requirement for the degree of Ph.D. in physics at the University of Chicago. Present address: Joseph Henry Laboratory,

Princeton University, Princeton, New Jersey 08540.
‖Present address: Department of Physics and Astronomy, University of New Mexico, Albuquerque, New Mexico 87106.
¶Present address: Brookhaven National Laboratory, Upton, New York 11973.

[1]J. Lindquist, R. L. Sumner, J. M. Watson, R. Winston, D. M. Wolfe, P. R. Phillips, E. C. Swallow, K. Reibel, D. M. Schwartz, A. J. Stevens, and T. A. Romanowski, Phys. Rev. Lett. 27, 612 (1971).
[2]B. Nelson, T. M. Knasel, J. Lindquist, R. L. Sumner, E. C. Swallow, R. Winston, D. M. Wolfe, J. M. Watson, P. R. Phillips, K. Reibel, D. M. Schwartz, A. J. Stevens, and T. A. Romanowski, Phys. Rev. Lett. 31, 901 (1973).
[3]E. P. Wigner, Phys. Rev. 73, 1002 (1948).
[4]G. Breit, Phys. Rev. 107, 1612 (1957).
[5]R. K. Adair, Phys. Rev. 111, 632 (1958).
[6]A. N. Baz' and L. B. Okun', Zh. Eksp. Teor. Fiz. 35, 757 (1958) [Sov. Phys.—JETP 8, 526 (1959)].
[7]R. H. Dalitz, *Strange Particles and Strong Interactions* (Oxford Univ. Press, London, 1962), p. 122.
[8]H. J. Votava and W. J. Thompson, Phys. Lett. 41B, 405 (1972).
[9]Philip Malmberg, Phys. Rev. 101, 114 (1956); H. W. Newson, R. M. Williamson, K. W. Jones, J. H. Gibbons, and H. Marshak, Phys. Rev. 108, 1294 (1957).
[10]S. M. Flatté, M. Alston-Garnjost, A. Barbaro-Galtieri, J. H. Friedman, G. R. Lynch, S. D. Protopopescu, M. S. Rabin, and F. T. Solmitz, Phys. Lett. 38B, 232 (1972).
[11]F. Eisler, P. Franzini, J. M. Gaillard, A. Garfinkel, J. Keren, R. Plano, A. Prodell, and M. Schwartz, Rev. Mod. Phys. 33, 436 (1961); F. Eisler, J. M. Gaillard, J. Keren, M. Schwartz, and S. E. Wolf, in *Proceedings of the Aix-en-Provence International Conference on Elementary Particles*, edited by E. Cremieu-Alcan, P. Falk-Vairant, and O. Lebey (C.E.N., Saclay, France, 1962), Vol. I, p. 203.
[12]S. E. Wolfe, N. Schmitz, L. J. Lloyd, W. Lasker, F. S. Crawford, Jr., J. Button, J. A. Anderson, and G. Alexander, Rev. Mod. Phys. 33, 439 (1961); J. A. Anderson, F. S. Crawford, B. B. Crawford, R. L. Golden, F. Grard, L. J. Lloyd, G. W. Meisner, L. R. Price, and G. A. Smith, *Proceedings of the International Conference on High Energy Physics, CERN, 1962*, edited by J. Prentki (CERN, Geneva, 1962), p. 270.
[13]J. Keren, Phys. Rev. 133, B457 (1964).
[14]J. J. Jones, T. Bowen, W. R. Dawes, D. A. Delise, D. W. Jenkins, R. M. Kalbach, E. I. Malamud, K. J. Neild, and D.V. Petersen, Phys. Rev. Lett. 26, 860 (1971).
[15]O. Van Dyck, R. Blumenthal, S. Frankel, V. Highland, J. Nagy, T. Sloan, M. Takats, W. Wales, and R. Werbeck, Phys. Rev. Lett. 23, 50 (1969).
[16]A. J. Stevens, D. M. Schwartz, C. J. Rush, K. Reibel, T. A. Romanowski, R. L. Sumner, E. C. Swallow, J. M. Watson, R. Winston, and D. M. Wolfe, Nucl. Instrum. Methods 97, 207 (1971). The momentum was calibrated at 997, 1007, 1018, and 1027 MeV/c.
[17]G. J. Marmer, K. Reibel, D. M. Schwartz, A. Stevens, P. R. Phillips, E. C. Swallow, R. Winston, D. M. Wolfe, T. A. Romanowski, and C. J. Rush, Phys. Rev. 179, 1294 (1969); Argonne National Laboratory Report No. ANL/HEP 6801, 1968 (unpublished).
[18]T. A. Romanowski, E. R. Hayes, J. Terandy, and K. Reibel, Nucl. Instrum. Methods 73, 117 (1969).
[19]R. L. Sumner, Nucl. Instrum. Methods 100, 371 (1972).
[20]D. Hodges, J. Lindquist, B. Nelson, E. C. Swallow, and D. M. Schwartz, Nucl. Instrum. Methods 108, 551 (1973).
[21]P. R. Phillips, Nucl. Instrum. Methods 75, 71 (1969).
[22]L. Baggett, thesis, Univ. of California, Berkeley, Report No. UCRL 8302, 1958 (unpublished).
[23]L. Bertanza, A. Bigi, R. Carrara, and R. Casali, Nuovo Cimento 44A, 712 (1966).
[24]G. Bizard, Y. Déclais, J. Duchon, J. L. Laville, J. Séguinot, C. Bricman, J. M. Perreau, and C. Valladas, Phys. Lett. 31B, 481 (1970).
[25]F. Bulos, R. E. Lanou, A. E. Pifer, A. M. Shapiro, C. A. Bordner, A. E. Brenner, M. E. Law, E. E. Ronat, F. D. Rudnick, K. Strauch, J. J. Szymanski, P. Bastien, B. B. Brabson, Y. Eisenberg, B. T. Feld, V. K. Kistiakowski, I. A. Pless, L. Rosenson, R. K. Yamamoto, G. Calvelli, F. Gasparini, L. Guerriero, G. A. Salandin, A. Tomasin, L. Ventura, C. Voci, and F. Waldner, Phys. Rev. 187, 1827 (1969).
[26]C. B. Chiu, R. D. Eandi, A. C. Helmholz, R. W. Kenney, B. J. Moyer, J. A. Poirier, W. B. Richards, R. J. Cence, V. Z. Peterson, N. K. Sehgal, and V. J. Stenger, Phys. Rev. 156, 1415 (1967).
[27]I. Derado and N. Schmitz, Phys. Rev. 118, 309 (1960).
[28]R. Turlay, thesis, Univ. of Paris Report No. C.E.A. 2136, 1962 (unpublished).
[29]L. Bertanza, P. L. Connolly, B. B. Culwick, F. R. Eisler, T. Morris, R. Palmer, A. Prodell, and N. P. Samios, Phys. Rev. Lett. 8, 332 (1962).
[30]L. B. Auerbach, D. Bowen, J. Dobbs, K. Lande, A. K. Mann, F. J. Sciulli, H. Uto, D. H. White, and K. K. Young, Nuovo Cimento 47, 19 (1967).
[31]P. Hargis, thesis, Univ. of Pennsylvania, 1972 (unpublished); G. Snape, thesis, Univ. of Pennsylvania, 1973 (unpublished).
[32]T. O. Binford, M. L. Good, V. G. Lind, D. Stern, R. Krauss, and E. Dettman, Phys. Rev. 183, 1134 (1969).
[33]J. C. Doyle, thesis, Univ. of California, Berkeley, Report No. UCRL 18139, 1969 (unpublished).
[34]J. A. Anderson, thesis, Univ. of California, Berkeley, Report No. UCRL 10838, 1963 (unpublished); and F. S. Crawford, M. Cresti, M. L. Good, K. Gottstein, E. M. Lyman, F. T. Solmitz, M. L. Stevenson, and H. K. Ticho, Phys. Rev. 108, 1102 (1957).
[35]For the proton asymmetry parameter in the $\Lambda \to p\pi^-$ decay ($\alpha = 0.646 \pm 0.016$) we use the average from the *Review of Particle Properties* [Particle Data Group, Phys. Lett. 39B, 1 (1972)].
[36]R. Bangerter, thesis, Univ. of California, Berkeley, Report No. UCRL 19244, 1969 (unpublished).
[37]J. E. Rush, Jr., Phys. Rev. 173 (1968).
[38]S. Orito and S. Sasaki, Nuovo Cimento 1, 936 (1969).
[39]F. Wagner and C. Lovelace, Nucl. Phys. B25, 411 (1971).
[40]H. Courant, H. Filthuth, P. Franzini, R. Glasser, A. Minguzzi-Ranzi, A. Segar, W. Willis, R. A. Burnstein, T. B. Day, B. Kehoe, A. J. Herz, M. Sakitt, B. Sechi-Zorn, N. Seeman, and G. A. Snow, Phys. Rev. Lett. 10, 409 (1963); C. Alft, N. Gelfand, U. Nauenberg, M. Nussbaum, J. Schultz, J. Steinberger, H. Brugger, L. Korsch, R. Plano, D. Berley, and

A. Prodell, Phys. Rev. 137, B1105 (1965).

[41]In general the coefficients of $|q|$ in Eq. (9) may be different above and below threshold (see Refs. 4 and 7). Although this damping parameter is not crucial to our fits, ξ takes on reasonable values ($\sim 0.7 m_\pi^{-1}$) with a small improvement is χ^2 ($\Delta\chi^2 = 2$ and 11 for solutions I and II).

[42]The $|\Sigma K, I = \frac{1}{2}\rangle$ cross section was calculated from the cross sections compiled by E. Bracci, J. P. Droulez, E. Flaminio, J. D. Hansen, and D. R. P. Morrison, CERN Report No. CERN/HERA 72-1, 1972 (unpublished).

[43]The χ^2 minimizing program is MINUIT from the CERN program library. The method is given by H. H. Rosenbrock, Comput. J. 3, 175 (1960).

[44]S. Almehed and C. Lovelace, Nucl. Phys. B40, 157 (1972). Note that $\Gamma_{\pi p} = \frac{2}{3}\Gamma_{\pi N}$.

[45]J. P. Baton, C. Coutures, O. Goussu, C. Kochowski, and M. Neveu, Proceedings of the Seventeenth International Conference on High Energy Physics, London, 1974, Session C4 [CEN-SACLAY report (unpublished)].